Program Digest, 2019 IEEE International Ultrasonics Symposium (IUS)
Glasgow, Scotland, October 6-9, 2019

Attenuation Compensation Comparison for Human Carotid Plaque Characterization Using Spectral Analysis of Backscattered Ultrasound

Sheronica James
Dept. of Biomedical Engineering
Cleveland Clinic
Cleveland, OH
jamess4@ccf.org

Russell Fedewa
Dept. of Biomedical Engineering
Cleveland Clinic
Cleveland, OH
fedewar@ccf.org

Sean Lyden
Dept. of Vascular Surgery
Cleveland Clinic
Cleveland, OH
lydenss@ccf.org

D. Geoffrey Vince
Dept. of Biomedical Engineering
Cleveland Clinic
Cleveland, OH
vinceg@ccf.org

***Abstract*— Carotid atherosclerotic plaque composition is a valuable predictor of stroke risk. Ultrasound spectral analysis has been successfully implemented clinically for determining plaque composition in coronary arteries via intravascular ultrasound. Noninvasive implementation for carotid plaque requires compensation for the attenuating effects of overlying tissue. This study examines the effects of four attenuation compensation techniques on the accuracy of a carotid plaque classification system using spectral analysis and random forest machine learning classification. Radiofrequency (RF) data was acquired from 20 subjects prior to carotid endarterectomy (CEA). 41 fibrous (F), 60 hemorrhagic and/or necrotic core (H/NC), and 54 calcified (Ca) regions of interest (ROI) were selected from the RF data corresponding to homogenous zones within the histology of the excised plaque tissue. Additionally, 219 ROI's were obtained from the adventitia (Adv) of six normal subjects. Power spectra for the ROI's were computed and normalized to a uniform phantom. Four attenuation compensation methods were applied to the spectra: (1) 0.5 dB/cm-MHz; (2) optimum power spectral shift estimator (OPSSE); (3) 1-step and (4) 2-step normalized backscatter from adventitia. A linear fit of the resulting estimated backscatter transfer functions (eBTF) was performed over the fundamental bandwidth of 2.5 – 6.9 MHz. Eight spectral parameters were used to build the random forest classification models. While there were no statistically significant differences in the accuracy of the classification models based off each attenuation compensation approach, our work has shown that additional attenuation compensation may provide a benefit for characterizing carotid plaque.**

***Index Terms*— Ultrasound, attenuation compensation, carotid plaque, tissue characterization**

I. INTRODUCTION

The ability to predict future cerebrovascular accidents (CVAs), such as stroke, in patients with carotid atherosclerosis is currently limited. While a high degree of carotid stenosis is the primary determining factor for selecting patients for carotid endarterectomy (CEA) to prevent stroke, the benefit of CEA in asymptomatic patients with high grade stenosis and symptomatic patients with a non-significant degree of stenosis is unclear.

Studies have shown that a large number of CVAs are caused by rupture-prone plaques with specific morphological features, regardless of degree of stenosis [1]–[3]. In carotid atherosclerosis, intra-plaque hemorrhage with a necrotic core distinguishes unstable, rupture-prone lesions from more stable ones. Thus, while plaque composition matters more than degree of stenosis in plaque rupture, it is generally unavailable at the point of care with current diagnostic tools.

While spectral analysis of intravascular ultrasound backscatter has been successfully implemented clinically for determining plaque composition in coronary arteries [4], [5], noninvasive implementation for carotid plaque characterization requires the ability to compensate the attenuation effects of overlying tissue in order to be sensitive to spectral parameters. This study examines the effects of four attenuation compensation techniques on characterizing human carotid plaque using spectral analysis and a random forest machine learning algorithm. Specific focus is placed on identifying hemorrhagic and/or necrotic core (H/NC) tissue, since this type of plaque tissue is most often associated with vulnerable or rupture-prone atherosclerotic lesions. An ultrasound-based technique that can noninvasively identify vulnerable lesions may aid in better risk stratification, particularly for asymptomatic patients and those with stenosis not considered clinically relevant.

II. HUMAN STUDY

A Siemens S3000 ultrasound system with Siemens Axius Direct Ultrasound Research Interface (URI) software was used to acquire beamformed RF data at a 40 MHz sampling rate from 20 subjects prior to carotid endarterectomy (CEA). Using a 9L4 linear array transducer, RF data was acquired in transverse slices approximately 1 cm apart throughout the plaque region. Histology slices of a portion of the excised plaque tissue obtained following removal during the CEA were prepared and matched to ultrasound frames. Regions of interest (ROI's), RF data points by 15 scanlines (~ 1.2 mm x 1.2 mm), were

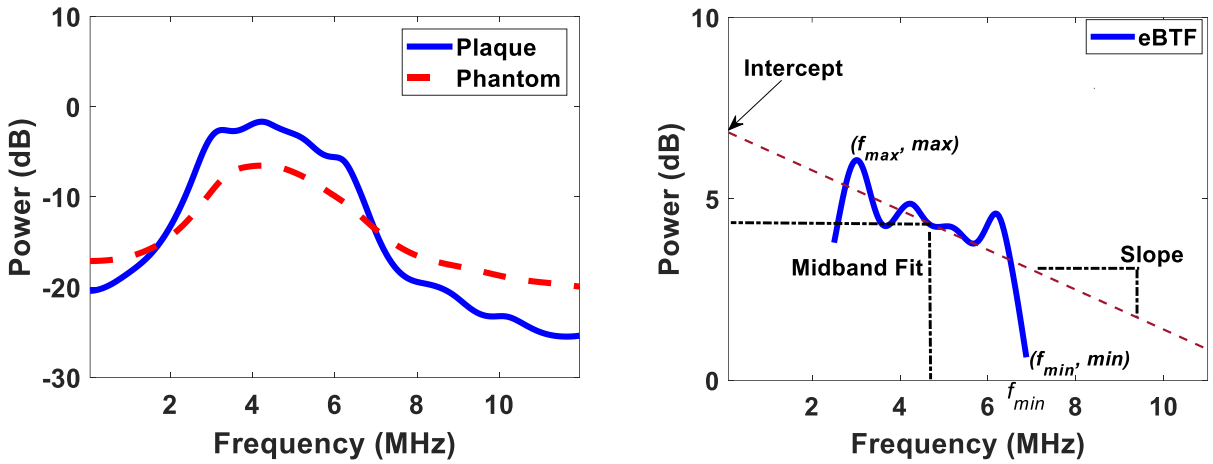

Fig. 1. Left – Sample average ROI power spectrum from plaque tissue and average reference phantom power spectrum. Right – eBTF within the usable 20dB down bandwidth of 2.5 -6.9 MHz. Linear fit parameters: slope, intercept and mid-band fit. Extreme points: maximum, minimum and corresponding frequencies. IB, a mean intensity parameter, was used

drawn in the RF data corresponding to homogenous zones within the matched histology slide. ROI's were categorized as F - fibrous (n = 41), H/NC - hemorrhagic and/or necrotic core (n = 60), or Ca - calcium (n = 54). Additionally, 209 ROI's were obtained from the adventitia (Adv) of six normal subjects.

III. SPECTRAL ANALYSIS

Under the assumptions of linear propagation, transmission and reception of the ultrasound wave, as well as single scattering (Born approximation) in a homogenous propagation medium, the power spectrum *S(f,d)* of a backscattered RF signal can be expressed as the product of the transmit and receive transfer function *G(f)*, diffraction effects *D(f,d),* attenuation from overlying tissue *A(f,d)*, and backscatter transfer function *B(f)*, represented as

$$S(f,d) = G(f) \cdot D(f,d) \cdot A(f,d) \cdot B(f,d). \quad (1)$$

Implementing spectral analysis to determine tissue composition requires separating the effects of the system, diffraction, and attenuation from the backscattered signal in order to be sensitive to the tissue properties. An autoregressive model (Yule-Walker, order = 24) was used to estimate an average power spectrum for each of the ROI's previously described. Below we discuss approaches to compensate for *G(f)*, *D(f,d)*, and *A(f,d)* to obtain an estimate of the backscatter transfer function (*eBTF*) that is robust and sensitive to the scattering properties of the target tissue within each ROI.

IV. ATTENUATION COMPENSATION METHODS

A. *Reference Phantom Method*

For *in vivo* applications in soft tissue, the reference phantom method has been demonstrated to effectively compensate for attenuation and diffraction effects, as well as the system transfer function [1]. Reference RF data was acquired from a 0.5 dB/cm-MHz phantom with identical transducer and system settings used to scan patients. A stable reference spectrum was obtained by averaging across 10 RF data frames and all scanlines. Each plaque ROI power spectrum was normalized to a reference power spectrum, $S_{ref}(f,d)$, corresponding to the same depth. An illustration of this normalization step is shown in figure 1. With the normalization step, the *eBTF* is defined as

$$eBTF(f,d) = \frac{S_{sam}(f,d)}{S_{ref}(f,d)} \quad (2)$$

where the subscripts *sam* and *ref* represent the tissue sample and reference phantom, respectively. In a homogenous medium with uniform attenuation properties, the cumulative overlying attenuation is expressed as

$$A(f,d) = e^{\{-4\beta \cdot f \cdot d\}}, \quad (3)$$

where β is the slope of attenuation expressed in dB/cm-MHz. Substituting (1) and (3) into (2),

$$eBTF(f,d) = \frac{B_{sam}(f,d)}{B_{ref}(f,d)} e^{4(\beta_s - \beta_R) f \cdot d}, \quad (4)$$

we see that the difference between the reference phantom attenuation and the attenuation of overlying tissue layers may still have an impact on the backscattered signals. While the *eBTF* does not need to be a perfect measure of the backscatter transfer function, it is desired that this robust approach permits the extraction of parameters sensitive to tissue properties. The following 3 attenuation compensation approaches were used to explore whether adding an additional attenuation compensation step to the phantom normalization improved our ability to characterize plaque tissue by enhancing separation of tissue properties.

B. *Optimum power spectral shift estimation*

The optimum power spectral shift estimator (OPSSE) [2], is

a correlation-based centroid shift estimator that improves upon the hybrid method [3] for estimating local attenuation coefficients in soft tissue. OPSSE provides an estimation of the center frequency shift with lower variance and higher stability compared to previous spectral shift methods [4], [5]. While the approach was initially used to isolate the scattering effects of the target tissue [2], we explore its use here as an attenuation compensation method to improve estimation of our power spectra by directly determining the attenuation of overlying tissue layers, β_R.

To calculate the attenuation of overlying tissue layers, RF data from a large window of interest (≈10mm x 5.5mm) was divided into 5 axially consecutive blocks with 75% overlap. An average power spectrum was calculated for each block and normalized to a reference phantom. Following normalization, a Gaussian filter with center frequency (f_c) and bandwidth (σ) similar to the transmit pulse,

$$G(f) = e^{\left\{-\frac{(f-f_c)^2}{2\sigma^2}\right\}}, \quad (5)$$

was applied to yield the Gaussian filtered normalized spectrum

$$GS(f,d) = e^{\left\{-\frac{(f-f_c)^2}{2\sigma^2}\right\}} \cdot \frac{B_{sam}(f,d)}{B_{ref}(f,d)}\, e^{4(\beta_s-\beta_R)f\cdot d}. \quad (6)$$

We estimated f_c and σ by fitting a 2-term Gaussian model to the received signal from the reference spectrum at the depth of the axial transmit focus. The 0.5 dB/cm-MHz attenuation was added back into the spectrum prior to fitting. Steps in rearranging Eq. (6), shown in previous work [4], [5], ultimately suggest that the normalized and Gaussian filtered spectrum will have a Gaussian form centered at

$$f_c = f - (\beta_s - \beta_R)d\sigma^2. \quad (7)$$

OPSSE correlates the Gaussian filtered normalized spectrum with the following weight to estimate the shift in center frequency.

$$B_{opt} = \frac{d}{df}\left(\frac{1}{G(f)}\right) \quad (8)$$

A linear least-squares fit of consecutive center frequency shift estimates along depth was used to calculate the attenuation coefficient of the tissue layers overlying the carotid artery.

C. *Adventitia-based attenuation compensation*

Adventitia has been used as a reference for tissue characterization [6]. Our adventitia-based attenuation compensation approaches use backscatter from the adventitia of normal subjects as a reference to compensate for attenuation differences between the reference phantom and tissue layers overlying the ROI's. 209 ROI's were selected from the adventitia of 6 normal subjects. An average power spectrum was estimated for each ROI and normalized to a uniform reference phantom. A linear least-squares regression model was obtained for each frequency within the fundamental bandwidth by fitting a line to the graph of *eBTF(f)* versus depth

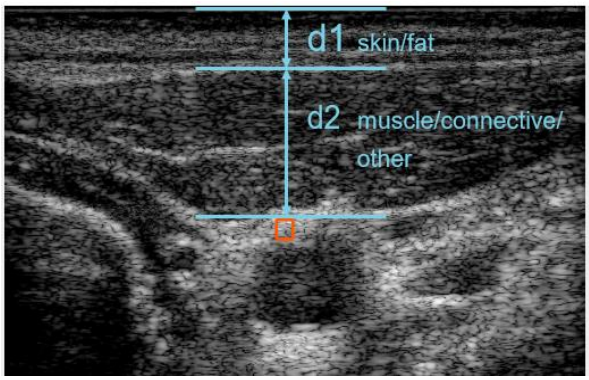

Fig 2. Sample grayscale image of a carotid artery from normal subject. Adventitia ROI in orange. The total depth of the ROI is the distance from the surface of the transducer to the starting edge of the ROI. Two layers of tissue comprise the total depth: (d1) skin/fat tissue and (d2) muscle, connective and other tissue.

for all 209 ROI's. For the one-step approach, depth was defined as the distance from the surface of the transducer to the starting edge of the ROI. The 2-step approach adds an additional parameter to the linear regression model by dividing the total depth into 2 layers, shown in figure 2: *d1*, skin and fat, and *d2*, the remaining muscle and other overlying tissue in the path to the ROI. An additional attenuation compensation was applied to each plaque ROI by inserting the ROI depth into the regression equations and subtracting the output from the *eBTF*.

D. *Random Forest Classification*

A linear least squares fit of the resulting eBTF was performed over the fundamental bandwidth of 2.5 MHz – 6.9 MHz, and a set of eight spectral parameters, shown in figure 1, were used to classify ROI's. These are slope, y-intercept, mid-band fit, integrated backscatter and the maximum and minimum powers with their corresponding frequencies [7]–[11].

A classification model for each data set was created using the MATLAB® *treebagger* [7] function, which implements the random forest algorithm [8]. Two-thirds of the data was randomly selected for training the model, while the remaining one third was used for cross-validation. The predicted outcomes of the cross-validation sets were compared to the known plaque types from histology to obtain the predictive accuracy, sensitivity and specificity of the classification models:

$$Predictive\ Accuracy = \frac{\text{All Correct Decisions}}{\text{Total Cases}} \quad (9)$$

$$Sensitivity = \frac{\text{True Positive Decisions}}{\text{Decisions Actually Positive}} \quad (10)$$

$$Specificity = \frac{\text{True Negative Decisions}}{\text{Decisions Actually Negative}} \quad (11)$$

An overall measure of agreement between the predictions and histology interpretation was determined by the Kappa statistic κ,

TABLE I
CLASSIFICATION SYSTEM ACCURACY

Attenuation Compensation Method	Kappa Statistic	H/NC Predictive Accuracy	H/NC Sensitivity		H/NC Specificity	
			%	CI	%	CI
0.5 dB/cm-MHz phantom	0.49	67%	55%	33-77	74%	59-90
OPSSE	0.52	69%	65%	44-86	71%	55-87
1-step adventitia-based	0.55	71%	60%	39-81	77%	63-92
2-step adventitia-based	0.70	80%	85%	69-100	77%	63-92

CI - 95% confidence interval

$$\kappa = \frac{n_a - n_\varepsilon}{n - n_\varepsilon}, \quad (12)$$

where n = number of samples, n_a = number of agreements and n_ε = number of agreements due to chance. The measure should fall between 0 and 1. Generally, a result of zero indicates low agreement (i.e. low predictive accuracy), while a test with $0.70 \leq \kappa \leq 1$ indicates a substantial to almost perfect agreement, with histology [9].

V. RESULTS

The accuracy assessment of each classification system was based on the confusion matrix constructed from the predicted and known values of each cross-validation data set. Plaque ROI's were classified into three types: Calcium (Ca); Fibrous/Fibro-Fatty (F); Hemorrhagic and/or Necrotic Core (H/NC). Results in Table I focus primarily on H/NC versus not H/NC, since this tissue type is associated with vulnerable or rupture-prone plaques. Four measures were considered: overall Kappa statistic, H/NC accuracy, H/NC sensitivity and H/NC specificity. While there were no statistically significant differences found in any of the methods to accurately classify the tissue types, the 2-step adventitia-based compensation does trend toward being the best overall, with a Kappa statistic of 0.70, 80% accuracy, 85% sensitivity. Specificity was similar for all attenuation compensation methods, between 71% and 77%.

VI. DISCUSSION

This study combined ultrasound spectral analysis with a random forest machine learning algorithm to classify carotid plaque tissue. Four attenuation compensation methods were compared for their effects on the accuracy of our classification system. Specific focus was placed on H/NC. The results of this study demonstrate that a reference phantom alone may be sufficient for attenuation compensation. However, this was a preliminary analysis with a small sample size. Thus, trends in the data appear to suggest that additional compensation beyond the 0.5 dB/cm-MHz based phantom attenuation may be beneficial. Obtaining a larger sample size and more importantly, comparing directly to histology is needed for a better comparison between compensation approaches. While ROI's used here were taken from homogeneous areas, plaques are heterogeneous by nature, and overlap between spectral parameter values is a likely source of inaccuracy in classification.

VII. CONCLUSION

A 0.5 dB/cm-MHz attenuation coefficient slope is a reasonable choice for attenuation compensation. Our work has shown that additional attenuation compensation may provide a benefit. Specifically, using adventitia as a reference shows promise. The final determination of the best attenuation compensation approach to use will depend on comparison to histology.

[1] L. Yao, "Reference Phantom Method for Acoustic Backscatter Coefficient and Attenuation Coefficient Measurements.," *PhD Thesis*, Aug. 1990.
[2] K. Samimi and T. Varghese, "Optimum Diffraction-Corrected Frequency-Shift Estimator of the Ultrasonic Attenuation Coefficient," *IEEE Trans. Ultrason. Ferroelectr. Freq. Control*, vol. 63, no. 5, pp. 691–702, 2016.
[3] H. Kim and T. Varghese, "Hybrid Spectral Domain Method for Attenuation Slope Estimation," *Ultrasound Med. Biol.*, vol. 34, no. 11, pp. 1808–1819, Nov. 2008.
[4] M. Fink, F. Hottier, and J. F. Cardoso, "Ultrasonic signal processing for in vivo attenuation measurement: short time Fourier analysis," *Ultrason. Imaging*, vol. 5, no. 2, pp. 117–135, Apr. 1983.
[5] R. Kuc and H. Li, "Reduced-order autoregressive modeling for center-frequency estimation," *Ultrason. Imaging*, vol. 7, no. 3, pp. 244–251, Jul. 1985.
[6] M.-H. Roy-Cardinal, F. Destrempes, G. Soulez, and G. Cloutier, "Assessment of Carotid Artery Plaque Components With Machine Learning Classification Using Homodyned-K Parametric Maps and Elastograms," *IEEE Trans. Ultrason. Ferroelectr. Freq. Control*, vol. 66, no. 3, pp. 493–504, 2019.
[7] "Create bag of decision trees - MATLAB." [Online]. Available: https://www.mathworks.com/help/stats/treebagger.html. [Accessed: 27-Aug-2019].
[8] L. Breiman, "Random Forests," *Mach. Learn.*, vol. 45, no. 1, pp. 5–32, Oct. 2001.
[9] A. J. Viera and J. M. Garrett, "Understanding interobserver agreement: the kappa statistic," *Fam. Med.*, vol. 37, no. 5, pp. 360–363, May 2005.